Experimental study on the effect of second order wavemaker theory on the response of a flexible large diameter monopile in irregular sea

Experimental study on the effect of second order wavemaker theory on the response of a flexible large diameter monopile in irregular sea

F H Dadmarzi[1], M Tonnel[2], M Thys[3], E E Bachynski-Polić[1] and T Kristiansen[1]
[1]Norwegian University of Science and Technology, NTNU, Trondheim, Norway
[2]Leopold-Franzens Universität Innsbruck, Innsbruck, Tyrol, Austria
[3]SINTEF Ocean, Trondheim, Norway

Abstract. Motivated by the need for larger offshore wind turbines, large diameter monopile foundations are being developed. To ensure safe design, there is a need for model testing and validation of hydrodynamic load models. Scaled model tests with a piston-type wavemaker commonly apply first order wavemaker theory for irregular waves. This approach results in the generation of second (and higher) order spurious (also known as parasitic) free waves in the tank. In this study, the effect of superharmonic spurious waves on the response of a monopile with eigenfrequency close to three times the wave peak frequency is examined experimentally. The bending moment response statistics are not found to be significantly affected by the wavemaker correction. Different wave breaking patterns are observed for individual events, but our results do not indicate any clear relation between breaking waves and the wave generation technique.

1. Introduction

The green shift in energy production has increased the industry interest in wind power. The number and size of monopile bottom-fixed offshore wind turbines has been increasing for the past decade. The increasing size of wind turbines introduces new challenges with respect to design and model testing. Accurate prediction of the responses of larger monopiles to nonlinear wave loads during extreme weather conditions, e.g. ringing [1] and slamming [2], is necessary for ultimate limit state (ULS) analysis and design. Model testing is an important tool for accurately estimating the loads and the responses of such monopile structures. There have been experimental studies on monopiles and response measurements in several projects such as WAS-XL [3], WiFi [2], WaveLoads [4].

Validation of numerical models based on experimental measurements requires knowledge of the uncertainties in model testing. One source of uncertainty is the wave generation technique. First-order wavemaker theory is well established, simple, and widely applied. Schäffer [5] presented a second order wavemaker theory for irregular waves, including both superharmonics and subharmonics for piston and hinged-type wavemakers. Spurious waves are free waves that are generated by mismatch of the velocity profile on the wavemaker when using linear wavemaker theory. A second order correction (based on second order wavemaker theory) can be used to suppress the generation of free spurious waves.

The correction of second order spurious waves for regular waves has already been tested in many experiments. For example, Kristiansen & Faltinsen's [6] study of the higher harmonic wave force on a cylinder in finite water depth also showed that the suppression of second order superharmonic spurious waves in the experiments gave better agreement with theory for the first three harmonics of the measured wave amplitude.

Sriram et al. [7] experimentally generated focused waves using linear and second order wavemaker theory with a piston-type wavemaker. For intermediate water depth, they observed a shift in focusing/breaking location and time (i.e. premature) due to the larger crest height using linear wavemaker theory.
Recently, Pierella et al. [8] numerically reconstructed superharmonic spurious waves using a phase separation technique in order to explain why the shape of wave spectra differs depending on distance from the wavemaker. They also used their numerical model to show that wave force maxima on a rigid monopile are not dramatically influenced by spurious waves (less than 10% difference for exceedance probabilities lower than 0.1).
Subharmonic spurious waves are mainly a concern in low-frequency horizontal motions of moored floating structures; this has been studied by, for example, Stansberg & Kristiansen [9] and Fonseca et al.[10]. For the present work, we focus on the superharmonic spurious waves because our structure has an eigenfrequency which is close to three times the wave peak frequency in ULS conditions.
We first present the methodology and experimental verification of the implementation of the second order wave generation correction. Then, we show the application of the correction to tests with representative sea states and a fully flexible monopile model.

2. Experimental setup

Two sets of experiments are included here: first, we verified the implementation of the second order wavemaker motion based on Schäffer's work [5], then we applied this correction in realistic sea states. Both sets of experiments were conducted in a medium size tank ("Lilletanken") at NTNU. At one end of the tank, there is a piston-type wavemaker and at the other end, an absorbing parabolic beach with adjustable height. The beach reflection (the amplitude of the reflected wave compared to the incident wave amplitude), is expected to be between 6 to 8% based on previous studies [11]. The tests using first and second order wavemaker theory are referred to as "without correction" and "with correction" in the paper, respectively. In both sets of experiments, the Froude scale is 1:50, and the water depth at full scale is 27 m. All results are presented at full scale unless otherwise noted.

2.1 Verification of the implementation

The basis for checking the implementation of the wavemaker motion correction is that the second order bound waves and the free spurious waves follow two different dispersion relations (Figure 1). This means that even though a free wave and a bound wave share the same frequency, they do not propagate with the same speed in the wave tank. This characteristic can be used to separate the spurious waves from the bound waves. By recording the wave elevation at different points in time and space, it is possible to decompose the wave signal using a 2D Fourier transform. Longer measurements with smaller increments (in space and time) give better resolution in such an analysis. Furthermore, due to the use of discrete measurements (in both space and time) and discrete Fourier transforms, we expect to see energy falling with a band rather than along the exact theoretical dispersion relation.

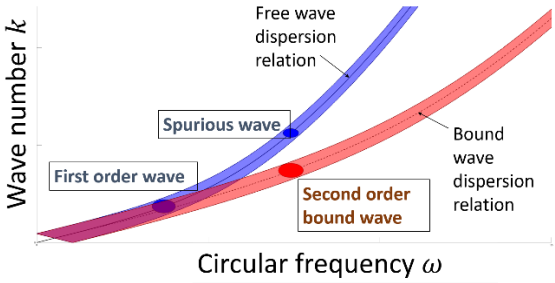

Figure 1. Schematic plot of dispersion relation for bound and free waves.

To obtain a sufficient resolution to be able to separate the bound wave and spurious wave, the wave elevation was measured over a length of 7 m with a step of 0.08 m (model scale). For practical reasons, it was not possible to measure the free-surface elevation at all the desired points simultaneously. The acquisition system for measuring the wave elevation was composed of 12 wave probes mounted on a harp and spaced 0.08 m from each other (Figure 2). The same wave was repeated 8 times. In between each run, the harp was moved to measure the elevation in another area of the tank. To check the

repeatability of the tests, four extra, stationary wave probes were included. Additionally, from one measurement of the same wave to another, the first wave probe of the harp was overlapped with the measurement point of the last wave probe of the previous run.

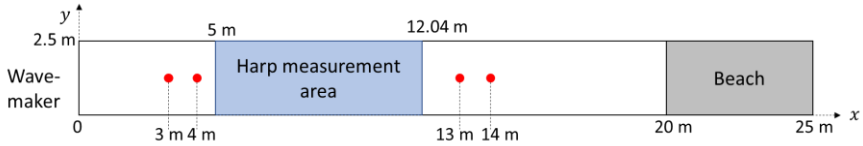

Figure 2. Tank top plan indicating the location of the wave probes and the photo of the harp with 11 wave probes (model scale).

The identification tests were performed for a narrow-banded wave spectrum in order to more easily distinguish the first-order and second-order free waves. Figure 3 shows the results of a test for a Gaussian spectrum with peak period $T_p = 12$ s, significant wave height $H_s = 4$ m and σ= 0.05 rad/s, where σ is used in the definition of the spectral width[12]. The Fourier transform with a rectangular window in space results in the appearance of parasitic lobes. Convoluting the signal with a Hamming window reduced those lobes but also widened the band in which the energy was located. In figure 3, different lines show different dispersion relations. The effect of the second order wavemaker motion correction can be seen in the circled location: there is a significant reduction of energy in the tests with correction.

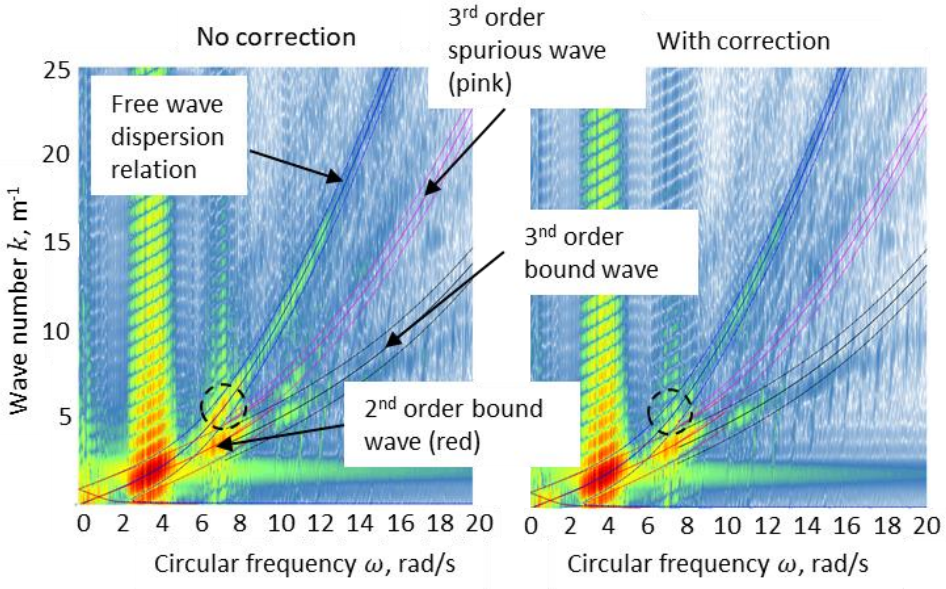

Figure 3. 2D Fourier transform of wave signal from tests without (left) and with correction (right) for a Gaussian spectrum with $T_p = 12$ s, $H_s = 4$ m, $\sigma = 0.05$ rad/s (full scale values). Results are shown at model scale (1:50). Lines show the dispersion relation for bound and free waves. The circle indicates the second order spurious wave peak energy. Warm colors represent higher energy/amplitudes on a linear scale.

Table 1. Tested Gaussian wave spectra parameters. In the last two columns, the relative energy of spurious wave to bound wave is listed for the tests without and with correction.

H_s (m)	T_p (s)	σ (rad/s)	steepness	Ratio spurious to bound second order wave	
				without correction	with correction
3	10	0.05	0.045	36%	7%
3	10	0.02	0.045	43%	6%
4	12	0.02	0.046	53%	26%
4	12	0.05	0.046	33%	6%

Table 1 summarizes the results of various tests with Gaussian spectra. The corresponding energy of the first and second order *bound* waves changed less than 0.5% and 0.9% from the test without correction to the test with correction. The last two columns of Table 1 show the reduction in the *spurious* wave energy with second order wavemaker correction. For some tests, we were not able to distinguish the spurious wave from the bound wave due to their overlap, which might explain why the correction does not seem to be completely effective. In addition, the correction requires high-frequency motion of the wavemaker, which may not always be achievable. A new wavemaker actuator-board, which was better able to follow high-frequency command signals, was installed for the model tests with the flexible monopile discussed in the next section. Despite these challenges, most of the tests with correction show a clear reduction from typically 30-40% to 6-7%, something that we judge as a significant improvement.

2.2 Tests with a flexible monopile

The model tests with the monopile wind turbine were performed in the same tank as the previously described tests (Figure 4). The tower and the monopile of a representative 10 MW monopile wind turbine are modelled using an elastic backbone model. The details of the model structure have been presented previously[3]. The first and second natural frequencies of the model are 0.25 and 1.58 Hz, and the first and second modes have critical damping ratios of 1.2% and 0.4%, respectively, based on wet decay tests. Three irregular sea-states were tested with and without correction, as summarized in Table 2. Most of the results presented in this paper are from the steepest sea state with significant wave height $H_s = 8.6$ m, and peak period $T_p = 11$ s.

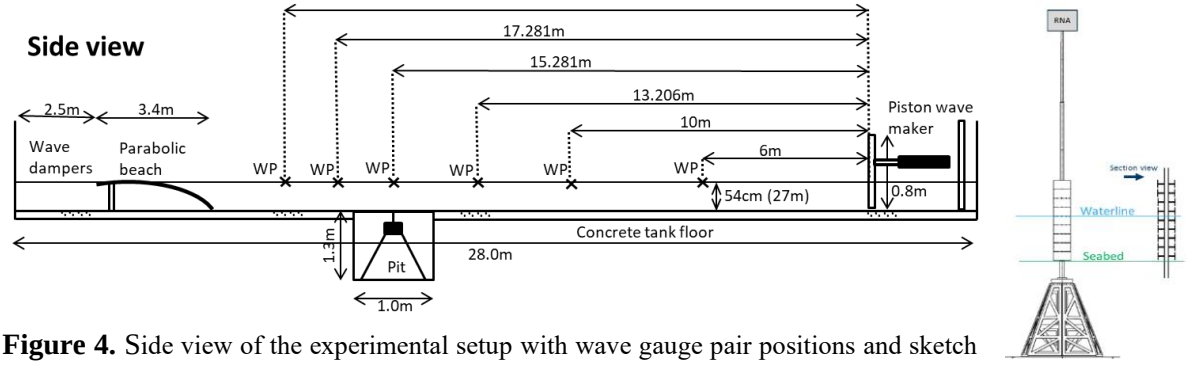

Figure 4. Side view of the experimental setup with wave gauge pair positions and sketch of the model construction (model scale).

Table 2. Irregular wave conditions with JONSWAP spectrum described by H_s, T_p, γ (peakedness parameter) and steepness. The two values of steepness for each sea state are calculated using both the linear and nonlinear dispersion relations. The steepness is defined as $s = H_s/\lambda$, where λ is the wavelength related to the peak period. One seed (one 3-hour wave realization) of the steepest sea states was repeated 10 times.

H_s (m)	T_p (s)	γ	steepness	No. of realizations	repetitions
8.6	11	4.2	0.057-0.059	19	10
9	12.5	2.6	0.050-0.052	10	
6.8	13.2	1	0.035-0.037	10	

3. Monopile model test results

3.1. Repeatability

To be able to evaluate whether differences between tests with and without correction fall within uncertainty bounds, the repeatability in the experimental results is briefly discussed here. One of the 3-hour realizations of the steepest sea state in the test without correction was repeated 10 times (Table 2). Figure 5 shows all the repetitions of two extreme bending moment events. Similar to Suja-Thauvin et al. [2], we have filtered the response into contributions near the first and second natural frequency. For brevity, these are referred to as first and second mode responses, respectively, and abbreviated as F1

and F2. The remaining part of the response is referred to as a quasi-static (QS) component, and responses at frequencies higher than the second natural frequency are not considered. The results show that the quasi-static responses have a high degree of repeatability. The responses at higher frequencies show some variations; for first mode response, the coefficient of variation (COV, standard deviation divided by mean) for the three sequential maxima shown in figure 5(a) is 5%, 3.8% and 4.6%. In the same figure, the second mode response in three sequential maxima has a COV of 8.7%, 10% and 12.3%.

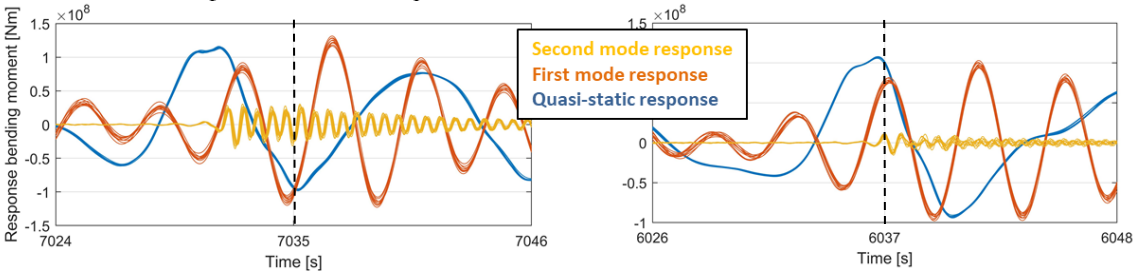

Figure 5. Repeatability of bending moment, including decomposition of bending moment for all repetitions. The time of the maximum response is indicated by dashed line. 10 repetitions are shown.

Figure 6 shows the COV for the contributions from each response component, at the exact time of maximum total response, for the 10 largest events in the 3-hour realization. The quasi-static responses have COV of less than 3%. The COV for the total bending moment and for the contribution near the first natural frequency is less than approximately 10%. The corresponding results for the responses near the second natural frequency are less than 70%, which is lower than the previous test campaign (more than 200%) [3]. The improved repeatability, especially in the response near the second natural frequency, is believed to be due to an upgrade in the laboratory wavemaker in between the two test campaigns, enabling better control at higher frequencies. Tank wall reflections and beach reflections, among others, might be reasons for the observed variations in the response. Further work is needed to understand these matters.

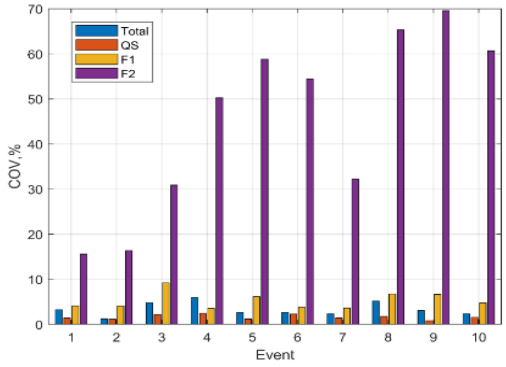

Figure 6. Coefficient of variation (COV) for the 10 largest bending moment maxima in 10 repetitions of one realization.

3.2. Wave measurements

The wave elevation spectrum for all 19 realizations in one of the sea states ($H_s = 8.6$ m and $T_p = 11$ s) for the tests without and with correction are shown in figure 7. The small differences between the signals with and without correction vary among different realizations, and the differences between the spectra with and without correction for a given realization are smaller than the differences among realizations. The mean measured wave spectra from both approaches are also shown in figure 7 with thicker lines. There are small differences between the tests with and without correction at the peak frequency (0.09 Hz) and twice the peak frequency (0.18 Hz). Similar behaviour was also seen for the other sea states.

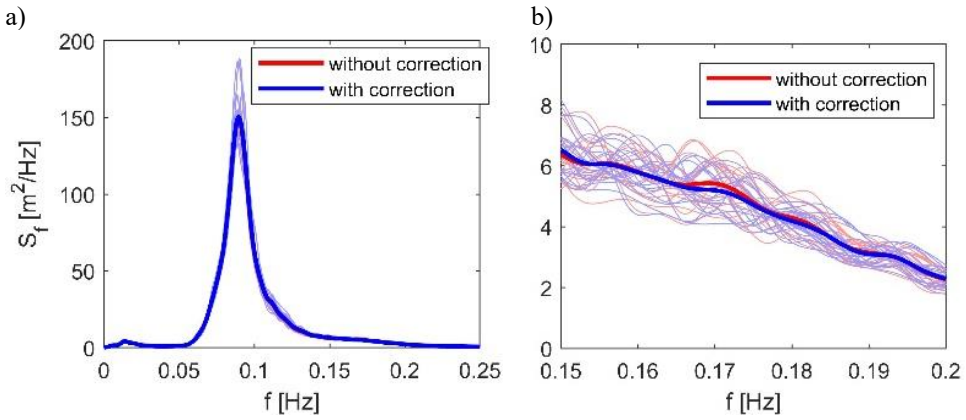

Figure 7. a) Power spectra of 19 3-hour realizations of the wave elevation (thin lines with light colors), together with calculated mean power spectra (thick lines with dark colors) are shown. (b) Zoomed view of main spectra around twice the wave peak frequency.

Figure 8 compares the empirical probability of exceedance for the wave elevation and (individual event) local steepness for 19 3-hour realizations of the steepest sea state ($H_s = 8.6$ m and $T_p = 11$ s) with and without correction. The local steepness in the present study is calculated based on the crest front amplitude and period (crest front height divided by wavelength, where the wavelength is calculated based on linear dispersion for intermediate water depth and the observed crest front half period). The correction has little effect on the main body of the tests ($P_{exceedance} > 0.01$). Except for one of the realizations in the test without correction, which has the largest extreme wave elevation and local steepness, the rest of the results stay within the range of sample variability. This suggests that the differences observed between the tests with and without correction are smaller than the spread in the extreme values in different realizations of each test.

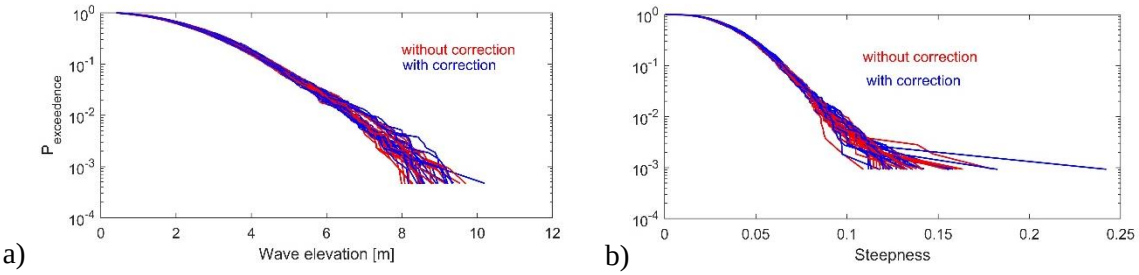

Figure 8. Exceedance probability of the wave elevation (a) and local wave steepness (b), for 19 3-hour realizations of a sea state. Red and blue lines are for the tests without and with the 2nd-order wavemaker correction, respectively.

3.3. Bending moment response

Figure 9(a,b) shows the power spectra of bending moment response for all 19 realizations of the same sea state together with the calculated mean power spectra for the tests with and without correction. Note that the term 'response' corresponds to the mudline bending moment for the flexible model. The wave peak frequency (0.09 Hz) corresponds to the largest peak in the spectra, while a small broad peak appears at twice the wave peak frequency (0.18 Hz). Additional peaks are present at the first (0.27 Hz) and second (1.56 Hz) natural frequencies of the structure. For individual realizations, the differences in the peaks of the spectrum between the realization without compared to with correction vary from -1.49% to 1.56% at the wave peak frequency, -13% to 20% at the first natural frequency and -47% to 28% at the second natural frequency. The differences in the mean spectra between the tests without and with correction are within the uncertainty of our test measurements.

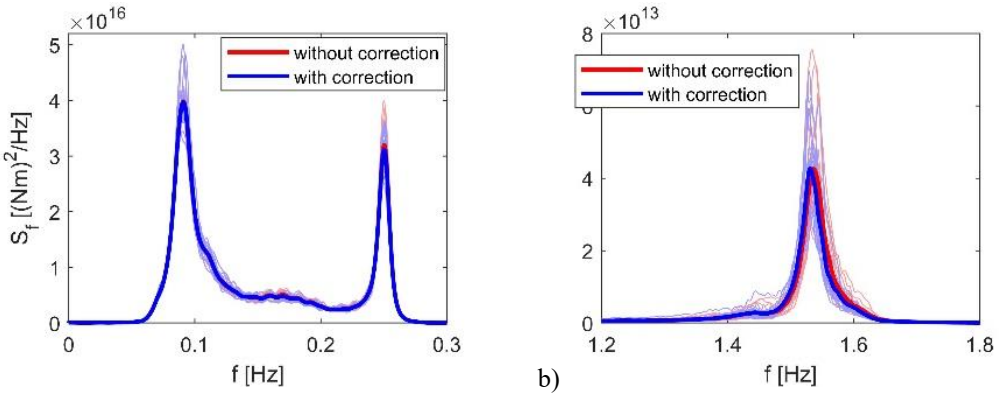

Figure 9. (a) Power spectra of 19 3-hour realization of the bending moment response (thin lines with light colors), together with calculated mean power spectra (thick lines with dark colors). (b) Zoomed view at the second natural frequency.

The probability of exceedance for the total measured response as well as first mode and second mode response, filtered and identified as in Figure 5, are presented in Figure 10. For $P_{exceedance} > 0.01$, the measured responses are very similar in both tests (without and with correction). There are deviations for larger responses between tests without and with correction, however, the observed spread among the realizations of each test is even larger. Moreover, our results show that the effect and importance of the correction varies from one realization to another. This might suggest a need for even larger number of realizations to better evaluate the effect of correction by reducing the spread due to sample variability. Our results do not support any significant variation in the statistical results by correcting the wavemaker motion up to second order. As previously mentioned, the first eigenfrequency of the model is about three times the peak frequency of the waves, and it is therefore not surprising that the second order wavemaker correction does not have a dramatic effect on the first mode response. Although removing second order spurious wave reduces third order spurious wave generation in the tank to some degree, the overall statistics of the first mode response did not change.
The largest differences are seen for the second mode response (between tests without and with correction), which also varies most significantly among different realizations.

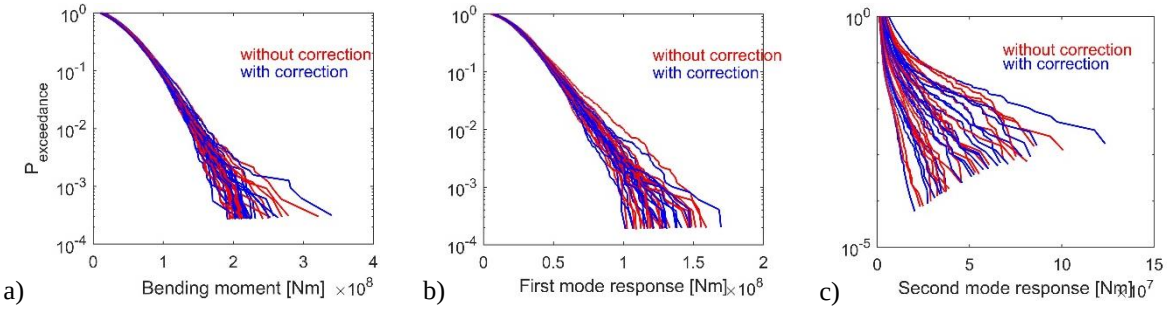

Figure 10. (a) Exceedance probability of the total mudline bending moment response, for 19 3-hour realizations of a sea state. (b-c) First and second mode response exceedance probability.

3.4. Individual maximum response event

Although the correction has little influence on the statistics of the response, there is an effect on individual events, and this is important for validation of numerical models. Four large events, identified based on the total measured response, have been chosen to discuss in this paper. The first event is the largest event in one of the three-hour realizations of the steepest sea state without correction. Snapshots of the wave at the location of the model for the tests with and without correction are shown in Figure 11, and the corresponding wave elevation at the model position (during calibration, without the model present) and response measurements for this event (at time 5771 s) are shown in Figure 12. Unlike the test without correction, the wave breaks before reaching the model for the test with correction, resulting

in a smaller bending moment response and smaller wave height. Both first and second mode responses are affected at this event due to observed breaking wave. Note that even without breaking, the two wave events (without and with correction) are in fact different. So one would expect different response also in a milder wave, that did not break (shown in the third event in the following).

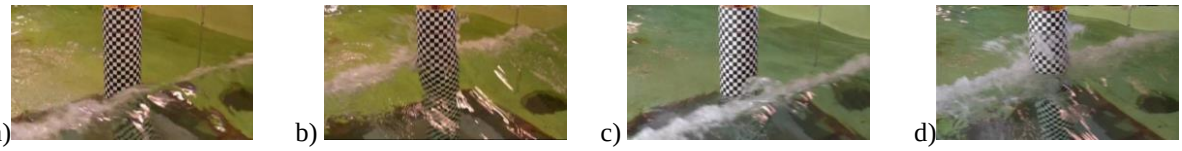

Figure 11. Event 1. Snapshot of the wave at the model location, for the test without correction (a,b) and with correction (c,d). The two snapshots of each tests (without and with correction) show two consecutive frames, corresponding to time instant 5771 s in Figure 12.

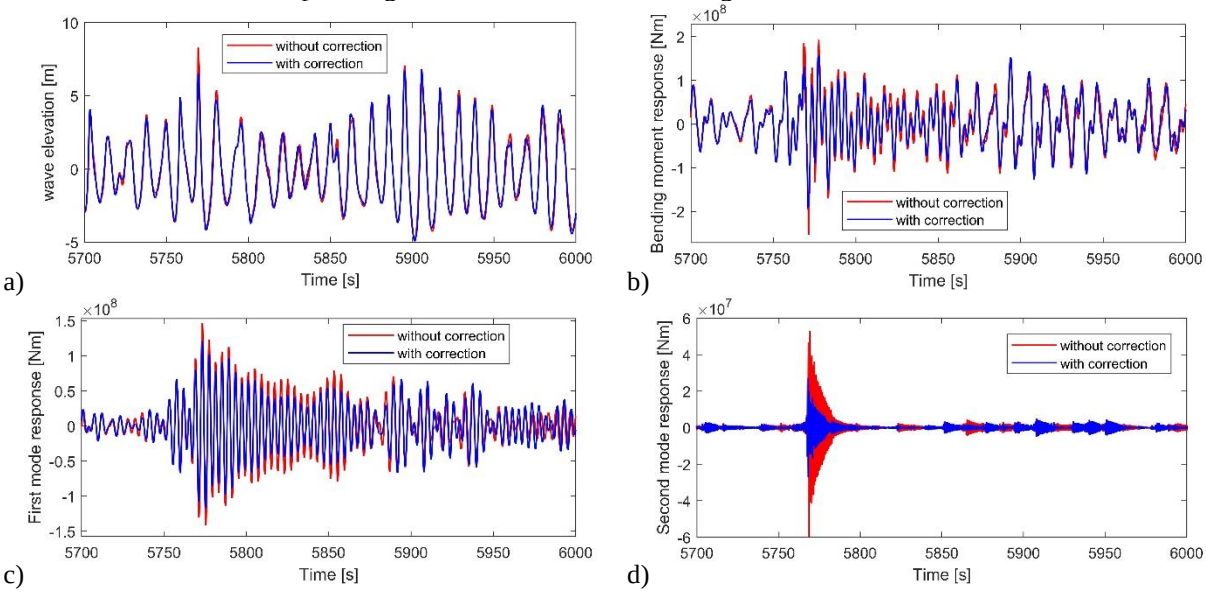

Figure 12. Wave elevation(a), total bending moment response (b) as well as first (c) and second (d) mode response ($f_1 = 0.25\ Hz$, $f_2 = 1.25\ Hz$). Event 1 occurs at time 5771 s, while Event 2 is at 5894 s.

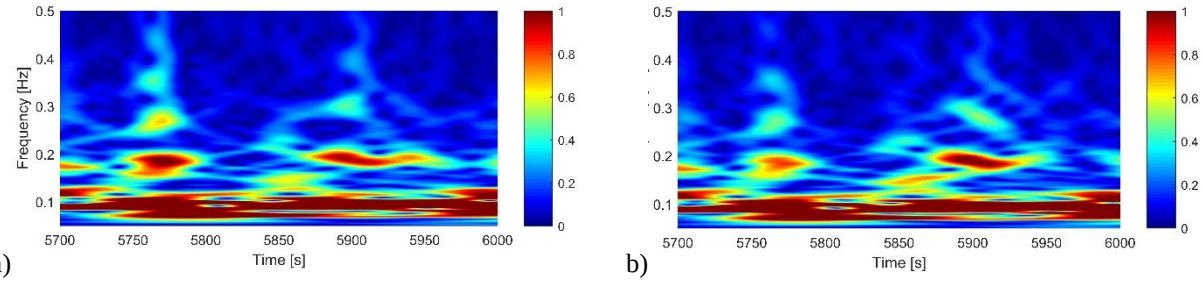

Figure 13. Wavelet analysis of the wave elevation (shown in figure 12(a)) for test without (a) and with (b) correction. Event 1 occurs at time 5771 s, while Event 2 is at 5894 s.

Due to the different propagation speeds of free spurious waves and bound waves, the presence of the spurious waves can cancel or enhance the wave energy in the second harmonic depending on the distance from the wavemaker in the wave tank. A wavelet analysis of the wave elevation can illustrate the temporal change in the amplitude (or energy) of the second harmonic of the wave, as shown in Figure 13. The bump wavelet function is used, and the coefficients are scaled to represent the amplitude of different components at each frequency. The total energy is not conserved in this method of scaling. The color bar indicates the amplitude of the wave signal at different frequencies.

The time window of the measured signals in Figure 12 and their wavelet analysis (Figure 13) correspond to two large events of the bending moment response. Event 1 at 5771 s is the largest response of this sea

state realization, while Event 2 at 5894 s is the 15th largest event. As shown, the wave amplitude at the peak frequency ($f_P = 0.09$ Hz) is similar in the test without and with correction, however, higher harmonics have different amplitudes. For Event 1 (time = 5771 s), the amplitude in the "peaks" at frequencies of 0.18 Hz, 0.27 Hz and 0.35 Hz are notably larger in the test without correction. However, in Event 2 (5894 s), the amplitude of the second harmonic (at $f_2 = 0.18$ Hz) is larger in the test with correction compared to test without correction. This can indicate an example of the cancellation effect of spurious waves in the tank. For Event 2, the peaks in third harmonic are not affected by the correction, and first mode responses are similar as well.

Event 3 is shown in Figure 14, without breaking waves. In this example, the local wave height and local steepness, as well as the response, are slightly larger in the test without correction. The difference is visible in the first and second mode responses. The local wave height and local steepness are 11.25 m and 0.0069 in the test without correction (with correction: 10.9 m and 0.066).

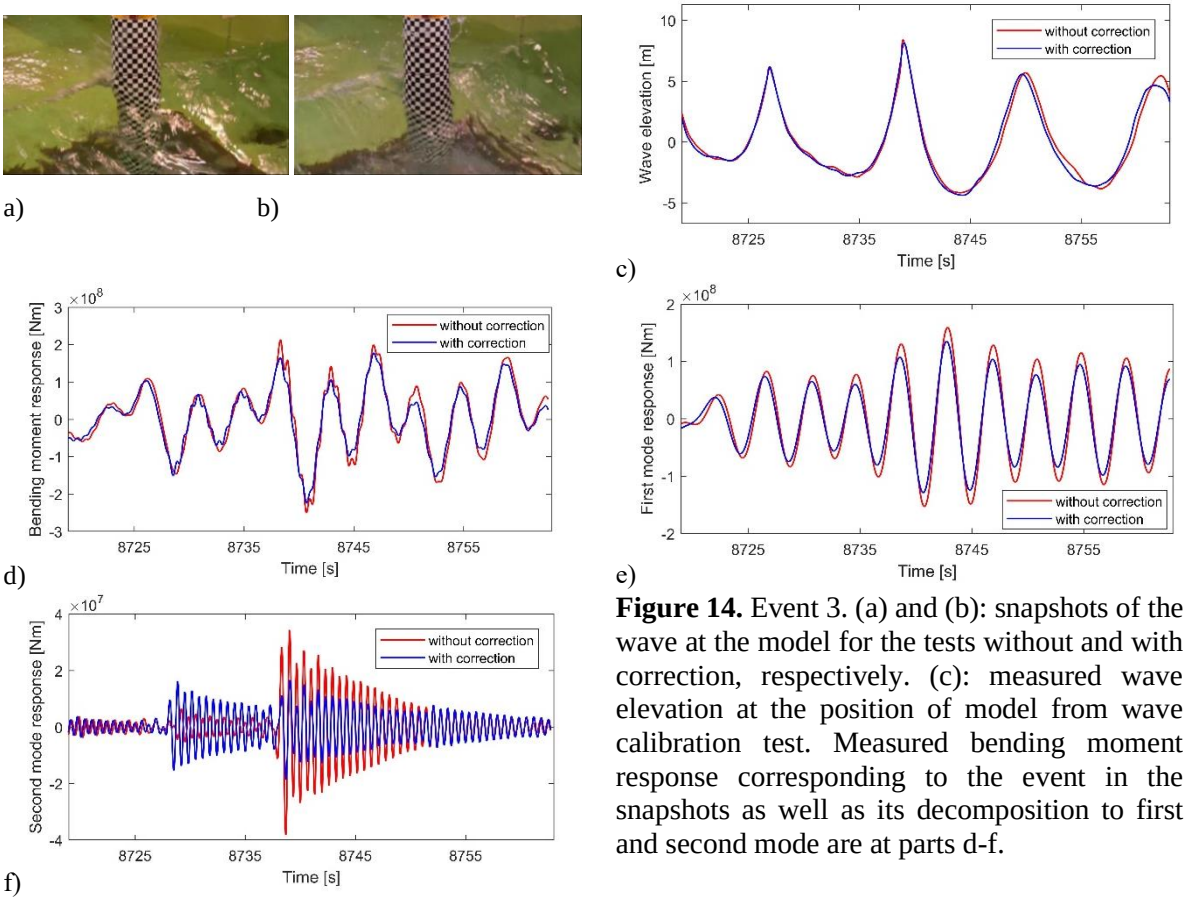

Figure 14. Event 3. (a) and (b): snapshots of the wave at the model for the tests without and with correction, respectively. (c): measured wave elevation at the position of model from wave calibration test. Measured bending moment response corresponding to the event in the snapshots as well as its decomposition to first and second mode are at parts d-f.

As shown in Figure 8.b, the correction does not affect the local wave steepness statistically, however, for individual events (for example Figure 14), different local steepnesses are seen for large wave episodes. To check the correlation between the local wave height, local steepness and bending moment response, these values for all 19 realizations of the sea state are plotted in figure 15. Here, the response maxima were chosen within each zero up-crossing of the wave elevation. The correlation between the response and local wave height and local steepness is similar in tests with and without correction. Responses larger than 1.5×10^8 Nm have probability of exceedance of less than 1%, as shown in figure 10(a). These responses are mainly seen for local wave steepnesses ranging from 0.03-0.15 and local wave height larger than 7 m for both tests (Figure 15). However, the density of these responses (warm colored scaled dots in figure 15) is a bit larger in the test without correction. Consistent with figure 10(a), the overall "warmer" color in the test without correction can be related to the three seeds with large responses in this test, compared to one seed in the test with correction (see also the exceedance probability plot, in figure 10(a)).

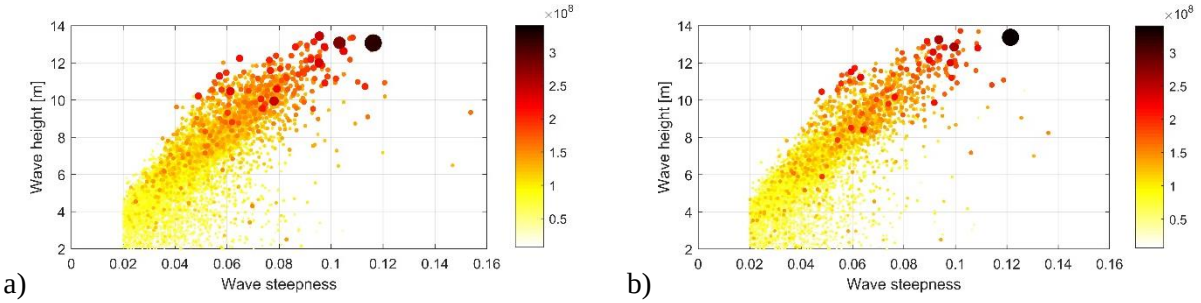

Figure 15. Scatter plot of local wave height vs. local wave steepness for tests without (left) and with (right) correction. The colorbar shows the bending moment response in Nm corresponding to each local wave height and local steepness, and the events with larger responses are marked with larger circles.

The last event, shown in Figure 16, is a breaking wave, chosen from the second steepest sea state with $H_s = 9$ m, $T_p = 12.5$ s. In this event, the wave with second order correction breaks at the model position and the corresponding monopile response is larger. The wave breaking results in a large second mode response, and the first mode response is also larger. Similar extreme breaking wave events happened in the tests without and with correction.

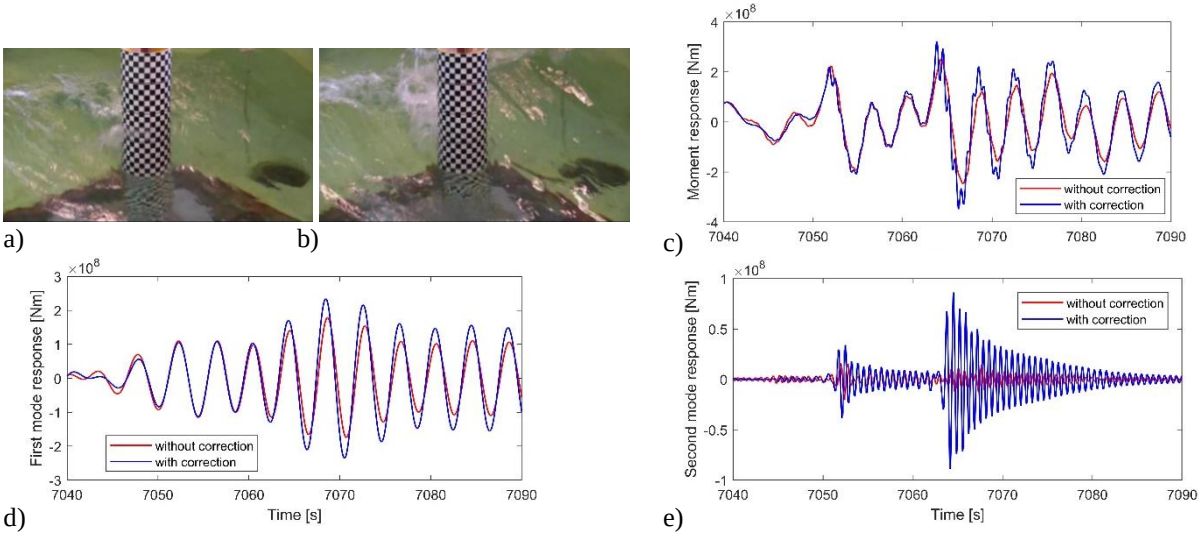

Figure 16. Event 4. Snapshots of the wave at the model location for the tests without (a) and with correction (b). The measured total response corresponding to the event in the snapshots is shown in subfigure (c). The response components, e.g. first mode and second mode responses, are in parts d-e.

4. Conclusions

Second order wavemaker theory for piston-type wavemaker motion in irregular waves based on Schäffer [5] was used to investigate the effects of superharmonic spurious wave generation on the response of a flexible monopile. Experimental measurements confirmed the reduction in the second order spurious wave component for narrow Gaussian spectra when using the second order. The main conclusions of this study are summarised as:

- Spurious (also known as parasitic) waves should preferably be removed in model tests due to better representation of real sea states (parasitic waves are artificial).
- For comparison with numerical codes/validation purposes, removal is beneficial.
- We observe significant differences in many large events (as expected).
- We cannot see any difference in the statistics of the results (not given, but not surprising).

Acknowledgments
The authors gratefully acknowledge the support from the Wave Loads and Soil Support for Extra Large

Monopiles (WAS-XL) project (NFR grant 268182).

References

[1] O. Faltinsen, *Sea Loads on Ships and Offshore Structures*, Cambridge University Press, **1993**.
[2] L. Suja-Thauvin, J. R. Krokstad, E. E. Bachynski, E.-J. de Ridder, *Ocean Eng.* **2017**, *146*, 339.
[3] E. E. Bachynski, M. Thys, F. H. Dadmarzi, *J. Phys. Conf. Ser.* **2020**, *1669*, 012028.
[4] H. Bredmose, P. Slabiak, L. Sahlberg-Nielsen, F. Schlütter, in *Vol. 8 Ocean Renew. Energy*, ASME, Nantes, France, **2013**, p. V008T09A062.
[5] H. A. Schäffer, *Ocean Eng.* **1996**, *23*, 47.
[6] T. Kristiansen, O. M. Faltinsen, *J. Fluid Mech.* **2017**, *833*, 773.
[7] V. Sriram, T. Schlurmann, S. Schimmels, *Appl. Ocean Res.* **2015**, *53*, 279.
[8] F. Pierella, *Coast. Eng.* **2021**, 14.
[9] C. T. Stansberg, T. Kristiansen, in *Vol. 3 Mater. Technol. Jan Vugts Symp. Des. Methodol. Offshore Struct. Jo Pinkster Symp. Second Order Wave Drift Forces Float. Struct. Johan Wichers Symp. Mooring Float. Struct. Waves*, ASME, Rotterdam, The Netherlands, **2011**, pp. 815–823.
[10] N. Fonseca, G. Tahchiev, S. Fouques, C. T. Stansberg, J. M. Rodrigues, American Society Of Mechanical Engineers Digital Collection, **2020**.
[11] T. Kristiansen, E. E. Bachynski, F. Bickert, A. Hniche, V. Kocher, A. Liandrat, in *Vol. 1 Offshore Technol.*, ASME, Trondheim, Norway, **2017**, p. V001T01A051.
[12] M. Olagnon, K. Ewans, G. Forristall, M. Prevosto, in *Vol. 2B Struct. Saf. Reliab.*, American Society Of Mechanical Engineers, Nantes, France, **2013**, p. V02BT02A029.